bioRxiv preprint doi: https://doi.org/10.1101/2023.04.06.535844; this version posted April 6, 2023. The copyright holder for this preprint (which was not certified by peer review) is the author/funder, who has granted bioRxiv a license to display the preprint in perpetuity. It is made available under a CC-BY-NC-ND 4.0 International license.

Progranulin inhibits phospholipase sPLA2-IIA to control neuroinflammation

Huan Du[1]*, Cha Yang[1]*, Alissa L. Nana[2], William W. Seeley[2,3], Marcus Smolka[1] and Fenghua Hu[1 #]

[1]Department of Molecular Biology and Genetics, Weill Institute for Cell and Molecular Biology, Cornell University, Ithaca, NY 14853, USA

[2]Department of Neurology, [3]Department of Pathology, University of California, San Francisco, CA 94158, USA.

WITHDRAWN
see manuscript DOI for details

*Running Title: PGRN regulates sPLA2-IIA to inhibit inflammation

* These authors contributed equally to the work.

#To whom correspondence should be addressed: Fenghua Hu, 345 Weill Hall, Ithaca, NY 14853, TEL: 607-2550667, FAX: 607-2555961, Email: fh87@cornell.edu

bioRxiv preprint doi: https://doi.org/10.1101/2023.04.06.535844; this version posted April 6, 2023. The copyright holder for this preprint (which was not certified by peer review) is the author/funder, who has granted bioRxiv a license to display the preprint in perpetuity. It is made available under a CC-BY-NC-ND 4.0 International license.

Abstract

Mutations in the granulin (*GRN*) gene, resulting in haploinsufficiency of the progranulin (PGRN) protein, are a leading cause of frontotemporal lobar degeneration (FTLD) and PGRN polymorphisms are associated with Alzheimer's disease (AD) and Parkinson's disease (PD). PGRN is a key regulator of microglia-mediated inflammation but the mechanism is still unknown. Here we report that PGRN interacts with sPLA2-IIA, a secreted phospholipase involved in inflammatory responses, to downregulate sPLA2-IIA activities and levels. sPLA2-IIA expression modifies PGRN deficiency phenotypes in mice and sPLA2-IIA inhibition rescues inflammation and lysosomal abnormalities in PGRN deficient mice. Furthermore, FTLD patients with *GRN* mutations show increased levels of sPLA2-IIA in astrocytes. Our data support sPLA2-IIA as a critical target for PGRN and a novel therapeutic target for FTLD-*GRN*.

Keywords: Progranulin, sPLA2-IIA, inflammation, lysosome, FTLD

WITHDRAWN
see manuscript DOI for details

bioRxiv preprint doi: https://doi.org/10.1101/2023.04.06.535844; this version posted April 6, 2023. The copyright holder for this preprint (which was not certified by peer review) is the author/funder, who has granted bioRxiv a license to display the preprint in perpetuity. It is made available under a CC-BY-NC-ND 4.0 International license.

Introduction

Progranulin (PGRN), encoded by the *granulin (GRN)* gene in humans, has emerged as a key player in brain aging and neurodegenerative diseases [1,2]. Mutations in the *GRN* gene, resulting in PGRN haploinsufficiency, are one of the major causes of frontotemporal lobar degeneration (FTLD) with TDP-43 positive inclusions [3-5]. Complete loss of PGRN in humans is known to cause neuronal ceroid lipofuscinosis (NCL) [6-8], a group of lysosomal storage diseases. *GRN* was also identified as one of the two main determinants of differential aging in the cerebral cortex [9] and as one of the five risk factors for limbic-predominant age-related TDP-43 encephalopathy (LATE) [10]. Polymorphisms in the *GRN* gene also contribute to the risk of Alzheimer's disease (AD)[11-14] and *GRN* is closely linked to Parkinson's disease (PD) [15,16].

PGRN is an evolutionarily conserved glycoprotein comprised of 7.5 granulin repeats [17-19] with critical roles in inflammatory responses [20]. PGRN is highly expressed in microglia, the resident immune cell in the brain, and regulates many aspects of microglial behavior [20]. PGRN deficiency results in exacerbated microglial activation, enhanced phagocytosis, increased levels of complement factors, and excessive synaptic pruning, leading to the disruption of brain circuits [21]. However, the mechanism by which PGRN affects brain inflammation is still unclear.

WITHDRAWN
see manuscript DOI for details

At the cellular level, PGRN is either secreted to the extracellular space or sorted into the lysosomal compartment within the cell [2,22]. PGRN is processed into granulin peptides in the lysosome and is critical for proper lysosomal functions, especially during aging, but the exact mechanisms by which PGRN regulates lysosomal activities remain to be fully dissected [2,22]. In addition, how PGRN functions extracellularly is still a mystery.

In this study, we show that PGRN interacts with a secreted phospholipase, sPLA2-IIA, and downregulates sPLA2-IIA activities to control brain inflammation and lysosomal phenotypes. sPLA2-IIA expression modifies phenotypes associated with PGRN loss and sPLA2-IIA inhibition rescues gliosis and lysosomal abnormalities in PGRN-deficient mice.

Results

PGRN physically interacts with sPLA2-IIA and regulates sPLA2-IIA levels

To understand the mechanisms of PGRN actions, we searched for PGRN interactors using a SILAC (stable isotope labeling by amino acids in cell culture) based proteomic screen (Fig. 1A). In addition to previously identified PGRN interactors, prosaposin (PSAP) [23] and folding chaperones (BIP, PDIA3, DJC10) [24], sPLA2-IIA (encoded by the *Pla2g2a* gene) was identified as one of the top hits from the screen (Fig. 1A, Supplementary Dataset 1). sPLA2-IIA is a secreted phospholipase of the sPLA2 family that catalyzes the hydrolysis of the sn-2 position of glycerophospholipids to generate fatty acids and lysophospholipids, many of which play a critical role in inflammation [25]. The PGRN/sPLA2-IIA interaction was further verified by co-immunoprecipitation (IP) with overexpressed human PGRN and sPLA2-IIA in both the medium and cell lysates (Fig. 1B). This interaction

bioRxiv preprint doi: https://doi.org/10.1101/2023.04.06.535844; this version posted April 6, 2023. The copyright holder for this preprint (which was not certified by peer review) is the author/funder, who has granted bioRxiv a license to display the preprint in perpetuity. It is made available under a CC-BY-NC-ND 4.0 International license.

is conserved with mouse PGRN and mouse sPLA2-IIA (Fig. 1C). PGRN and sPLA2-IIA colocalize with the Golgi marker ACBD3 when overexpressed, consistent with both of them being secreted proteins synthesized in the secretory pathway (Fig. S1A). Co-IP experiments with individual granulin peptides expressed as GFP fusion proteins indicate that granulins F and G have a high affinity for sPLA2-IIA (Fig. 1D,1E). However, the deletion of granulins F and G significantly reduced but not abolished the interaction between PGRN and sPLA2-IIA (Fig. 1F), suggesting that other granulins besides granulins F and G can also bind to sPLA2-IIA weakly.

Next, we determined the functional significance of PGRN interaction with sPLA2-IIA. To test whether PGRN could directly regulate sPLA2-IIA activities, we purified recombinant sPLA2-IIA from the medium of transfected HEK293T cells and performed in vitro assays with colorimetric substrates of sPLA2 in the absence or presence of recombinant PGRN. We found that the presence of PGRN significantly reduced the activity of sPLA2-IIA at 1:1 and 1:2 molar ratios compared to the control reaction with sPLA2-IIA alone or with sPLA2-IIA and bovine serum albumin (BSA) at 1:1 ratio (Fig. 2A).

To determine whether PGRN could also regulate sPLA2-IIA levels, we examined sPLA2-IIA levels in the cell lysate and medium of Raw264.7 macrophage cells with PGRN expression reduced by CRISPR. We found that the levels of sPLA2-IIA are significantly increased in the medium but not in the cell lysates of PGRN deficient Raw264.7 cells (Fig. 2B,2C). *Pla2g2a* mRNA levels are not changed in PGRN deficient Raw264.7 cells based on RT-qPCR analysis (Fig. 2D), suggesting that PGRN regulates sPLA2-IIA levels post-transcriptionally. The addition of recombinant PGRN in the medium leads to a reduction of extracellular sPLA2-IIA levels in both control and PGRN deficient cells (Fig. 2B,2C). Since PGRN trafficks to lysosomes and is critical for proper lysosomal functions [22], we hypothesized that PGRN might downregulate sPLA2-IIA by targeting it for lysosome degradation. However, we failed to detect any alterations in endogenous sPLA2-IIA levels in Raw264.7 cells with lysosomal activities inhibited (Fig.S1B).

WITHDRAWN
see manuscript DOI for details

sPLA2-IIA modifies the phenotypes associated with PGRN loss in mouse models

Since sPLA2-IIA is an important mediator of inflammation through the generation of arachidonic acids (AAs) and other fatty acid signaling molecules [25-27], we hypothesized that PGRN might regulate inflammation through sPLA2-IIA. The commonly used mouse strain C57BL/6 (B6) harbors a mutation in *Pla2g2a*, which leads to the loss of the sPLA2-IIA protein [28] (Fig. S2). To determine the role of sPLA2-IIA in PGRN deficiency phenotypes, we crossed $Grn^{-/-}$ mouse strain in the C57BL/6 background with wild-type (WT) FVB mice, which expresses WT *Pla2g2a* (Fig. S2). Brain pathology was examined in mice with two WT alleles of *Pla2g2a* ($Pla2g2a^{+/+}$) with or without PGRN deletion in the FVB/B6 hybrid background to determine the consequences of PGRN loss. Interestingly, we found a significant increase in lipofuscin accumulation, and glial activation in the 5-month-old $Pla2g2a^{+/+}$ $Grn^{-/-}$ mice (Fig. S3). This phenotype can also be observed in the 2-month-old $Pla2g2a^{+/+}$ $Grn^{-/-}$ mice in the FVB/B6 background (Fig. 3A, 3B). To further confirm this phenotype, we backcrossed $Grn^{-/-}$ mice into the FVB background for additional 6 generations and compared lipofuscin signal and glial activation in the 2-month-old $Pla2g2a^{+/+}$ $Grn^{-/-}$ mice with littermate WT controls. Similar increases in lipofuscin accumulation and

bioRxiv preprint doi: https://doi.org/10.1101/2023.04.06.535844; this version posted April 6, 2023. The copyright holder for this preprint (which was not certified by peer review) is the author/funder, who has granted bioRxiv a license to display the preprint in perpetuity. It is made available under a CC-BY-NC-ND 4.0 International license.

glia activation were observed (Fig. S4A). Since PGRN loss does not lead to any obvious microglia activation and lipofuscin accumulation in the 2-month-old C57BL/6 mice which do not express sPLA2-IIA (Fig. S4B) and the phenotype only becomes obvious in 9-10 months old [29], our data support that the expression of sPLA2-IIA greatly accelerates the phenotypes associated with PGRN loss. This indicates that regulation of sPLA2-IIA by PGRN could play an important role in restricting brain inflammation and lipofuscin accumulation.

To further determine the effect of PGRN loss in sPLA$_2$-IIA expressing background, we performed RNA seq analysis with RNAs isolated from cortical regions of 5-month-old *Pla2g2a*$^{+/+}$ mice with or without PGRN expression. Consistent with published results and a critical role of PGRN in the lysosome [22] and inflammation [20], lysosome and inflammation pathways are among the most upregulated pathways upon PGRN loss in the *Pla2g2a*$^{+/+}$ background (Fig. 4A-4C, and Dataset 2). To further characterize changes in lysosomal phenotypes in microglia, we immunostained 2-month-old *Pla2g2a*$^{+/+}$ and *Pla2g2a*$^{+/+}$ *Grn*$^{-/-}$ mice with antibodies against lysosomal proteins, LAMP1, and cathepsin D, together with microglial marker IBA1. A significant increase in the levels of LAMP1 and cathepsin D was detected in PGRN deficient microglia (Fig. 5A, 5B). In addition, enlarged lysosomes are frequently found in PGRN deficient NeuN+ neurons but not in the GFAP+ astrocytes (Fig. 5C), supporting early lysosomal defects in both microglia and neurons upon PGRN loss in the *Pla2g2a*$^{+/+}$ mice.

WITHDRAWN
see manuscript DOI for details

Since PGRN haploinsufficiency is a leading cause of FTLD, we also examined the phenotype of *Pla2g2a*$^{+/+}$ *Grn*$^{+/-}$ mice. No obvious inflammation and lysosomal phenotypes were observed in these mice at 5-month-old (Fig. S5), indicating that partial loss of PGRN is not sufficient to induce inflammatory and lysosomal abnormalities at this age even when *Pla2g2a* is expressed.

sPLA2-IIA inhibitors rescue phenotypes associated with PGRN loss in mouse models.

To determine whether sPLA2-IIA alterations are responsible for the inflammation and lysosomal phenotypes in PGRN deficient mice in the FVB background, we treated 5-week-old *Pla2g2a*$^{+/+}$ *Grn*$^{-/-}$ mice with LY333013, a broad inhibitor of the sPLA2 family phospholipases, or KH064, a specific inhibitor of sPLA2-IIA [26]. Strikingly, inhibition of sPLA2-IIA not only rescues the microgliosis and astrogliosis phenotypes but also lipofuscin accumulation in *Grn*$^{-/-}$ mice in the *Pla2g2a*$^{+/+}$ background (Fig. 6A, 6B). Enlarged lysosomes and increased levels of cathepsin D in neurons and microglia of *Pla2g2a*$^{+/+}$ *Grn*$^{-/-}$ mice are also rescued by treatment with sPLA2-IIA inhibitor (Fig. 7A, 7B). These results support that the increase in the sPLA2-IIA activities results in enhanced inflammation and lysosomal abnormalities in the *Pla2g2a*$^{+/+}$ *Grn*$^{-/-}$ mice.

Increased sPLA2-IIA levels in human FTLD patients with *GRN* mutations

To determine whether sPLA2-IIA levels are affected in FTLD patients with *GRN* mutations, we analyzed sPLA2-IIA levels in the lysates of the anterior orbital gyrus region by ELISA. A significant increase in sPLA2-IIA levels was found in patients with FTLD-TDP and carrying a GRN mutation (FTLD-*GRN*) but not in FTLD patients with corticobasal degeneration (CBD) positive with Tau aggregates (FTLD-Tau) (Fig. 8A) (Table S1).

bioRxiv preprint doi: https://doi.org/10.1101/2023.04.06.535844; this version posted April 6, 2023. The copyright holder for this preprint (which was not certified by peer review) is the author/funder, who has granted bioRxiv a license to display the preprint in perpetuity. It is made available under a CC-BY-NC-ND 4.0 International license.

To investigate the cellular distribution of sPLA2-IIA, we immunostained human brain sections with sPLA2-IIA antibodies. We found that elevated sPLA2-IIA signals in GFAP positive astrocytes in FTLD-*GRN* patients, indicating that sPLA2-IIA is highly expressed by astrocytes in FTLD patient samples with *GRN* mutations (Fig. 8B).

Discussion

PGRN regulates sPLA2-IIA activities and levels

In this study, we have identified sPLA2-IIA as a novel interactor for PGRN and shown that PGRN inhibits sPLA2-IIA activities and downregulates its levels to regulate neuroinflammation. Our results indicate that PGRN regulates sPLA2-IIA through two different mechanisms: (1) PGRN inhibits sPLA2-IIA activities through direct protein-protein interaction (Fig. 1B, 1C, and 2A); (2) PGRN downregulates extracellular sPLA2-IIA levels (Fig. 2B, 2C). It is unclear how PGRN regulates sPLA2-IIA levels at this point. Since PGRN is a lysosomal protein, we have hypothesized that PGRN might downregulate sPLA2-IIA by targeting it for lysosome degradation. However, we fail to detect any alterations in sPLA2-IIA levels with lysosomal activities inhibited (Fig. S1B). Another possibility is that PGRN might promote the degradation of sPLA2-IIA in the extracellular space by regulating the activities of proteases. In this regard, PGRN has been shown to interact with the secretory leukocyte protease inhibitor (SLPI) [30], a disintegrin and metalloproteinase with thrombospondin motifs 7 and 12 (ADAMTS-7 and 12) [31,32], and matrix metalloproteinase (MMP)-12 [33]. Future studies are needed to dissect the mechanism by which PGRN regulates sPLA2-IIA levels.

WITHDRAWN
see manuscript DOI for details

sPLA2-IIA is a member of a secreted PLA2 protein family (sPLA2), which catalyzes the hydrolysis of the sn-2 position of glycerophospholipids and is an important mediator of inflammation through the generation of arachidonic acids (AAs) and other fatty acid signaling molecules [25-27]. There are 11 family members of sPLA2, each of which has different tissue-specific expression patterns and slight differences in substrate specificity [25-27]. Interestingly, the presence of sPLA2-IIA in the FVB but not C57BL/6 background greatly modifies PGRN deficiency phenotypes, and the specific inhibitor of sPLA2-IIA, KH064, rescues glial activation and lysosomal abnormalities associated with PGRN loss, indicating that the activity of sPLA2-IIA is more critical in the development of phenotypes associated with PGRN loss compared to other sPLA2 family members. However, we can not rule out the possibility that other differences in the FVB and B6 strain background could work together with sPLA2-IIA to modify PGRN deficiency phenotypes.

sPLA2-IIA and inflammation

Interestingly, sPLA2-IIA levels are low in the mouse brain and undetectable in our studies (Fig. S6A). The highest level of $sPLA_2$-IIA expression is found in the gut (Fig. S6A) and $sPLA_2$-IIA has been shown to regulate gut microbiotome, inflammation and metabolism [34-36]. It also has been demonstrated to function as an intestinal stem cell niche factor to regulate intestine homeostasis, inflammation, and cancer [37]. An increase in sPLA2-IIA levels in the duodenum was found under PGRN deficient conditions (Fig. S6B,S6C). Alteration in the gut has

bioRxiv preprint doi: https://doi.org/10.1101/2023.04.06.535844; this version posted April 6, 2023. The copyright holder for this preprint (which was not certified by peer review) is the author/funder, who has granted bioRxiv a license to display the preprint in perpetuity. It is made available under a CC-BY-NC-ND 4.0 International license.

been shown to affect brain pathology through many different mechanisms [38,39]. Thus it is possible that PGRN regulates brain inflammation phenotypes by modulating sPLA2-IIA function and levels in the gut. However, although sPLA2-IIA levels are low in the brain, studies have shown that sPLA2-IIA is expressed by astrocytes [40,41] and endothelial cells [42]. We have also detected increased levels of sPLA2-IIA in FTLD-*GRN* patients and sPLA2-IIA seems to be increased specifically in astrocytes (Fig. 8). Secreted sPLA2-IIA has been shown to cause neuronal toxicity [41], stimulate phagocytosis, proliferation, and inflammatory responses of microglia-derived BV2 cells [43], and proliferation of an astrocytoma cell line [44]. sPLA2-IIA levels are increased after spinal cord injury and sPLA2-IIA has a detrimental effect [45]. In addition, sPLA2-IIA mRNA is up-regulated in Alzheimer's disease (AD) brains and sPLA2-IIA-immunoreactive astrocytes are associated with amyloid β (Aβ)-containing plaques in AD [46]. Oligomeric Aβ1-42 and interleukin-1β (IL-1β) were shown to induce sPLA2-IIA mRNA expression [46]. Thus, although sPLA2-IIA levels are low in the brain, brain-expressed sPLA2-IIA might be still subject to regulation by PGRN to regulate brain inflammatory phenotypes. Future studies are needed to pinpoint the actions of PGRN and sPLA2-IIA in the periphery versus in the brain.

Since sPLA2-IIA is a secreted enzyme, hydrolysis of lipids in the extracellular vesicles or the extracellular leaflet of the plasma membrane will lead to the production of AAs and other inflammatory lipid mediators, such as prostaglandins [25-27]. However, sPLA2-IIA has been shown to have catalytic independent functions, such as signaling through its receptors [25-27]. PGRN might regulate other functions of sPLA2-IIA in addition to its catalytic activities to modulate inflammation and lysosomal phenotypes.

WITHDRAWN
see manuscript DOI for details

Connections between inflammation and lysosomal abnormalities

Intriguingly, sPLA2-IIA expression not only modifies glial inflammation but also lysosomal abnormalities and lipofuscin accumulation and sPLA2-IIA inhibitors rescue both lipofuscin accumulation and lysosomal abnormalities under PGRN deficient conditions. While the mechanisms by which sPLA2-IIA regulates lysosomal phenotypes remain to be investigated, many recent studies have established a close link between lysosomal dysfunction and inflammation. For example, lysosomal membrane permeability (LMP) often results in the release of lysosomal enzymes and substrates into the cytosol, which often leads to inflammasome activation [47-49]. In addition, the activation of TFE3/TFEB, the transcriptional factors involved in lysosome biogenesis, has been shown to drive the expression of not only lysosomal genes but also inflammation genes in several studies [50,51]. Furthermore, substrate accumulation and lysosome stress can activate Stat3, which is known to mediate the transcription of many genes involved in inflammatory responses [52]. However, while sPLA2-IIA is important for inflammatory responses by producing lipid mediators of inflammation, its role in the lysosomal compartment is completely unexplored. sPLA2-IIA might affect lysosomal activities indirectly through modulating lipid signaling and lipid composition through its catalytic activities, signaling functions or it might regulate lysosomal functions through other mechanisms.

sPLA2-IIA as a novel therapeutic target for FTLD-*GRN*

bioRxiv preprint doi: https://doi.org/10.1101/2023.04.06.535844; this version posted April 6, 2023. The copyright holder for this preprint (which was not certified by peer review) is the author/funder, who has granted bioRxiv a license to display the preprint in perpetuity. It is made available under a CC-BY-NC-ND 4.0 International license.

PGRN has emerged as a hot target to treat neurodegenerative diseases [1,2]. Our studies support the important role of sPLA2-IIA in FTLD-*GRN* pathogenesis. sPLA2-IIA expression strongly modifies phenotypes associated with PGRN deficiency in mouse models and sPLA2-IIA inhibition rescues inflammation and lysosome phenotypes associated with PGRN loss in the sPLA2-IIA expressing background. Our results support that sPLA2-IIA is a critical target of PGRN action and suggest that inhibition of sPLA2-IIA might be a valid therapeutic approach for FTLD-*GRN*, and possibly also other neurodegenerative diseases to restrict neuroinflammation.

WITHDRAWN
see manuscript DOI for details

Material and Methods

DNA and Plasmids

Human *Pla2g2a* cDNA in the pDONR221 vector was obtained from DNASU. Human *Pla2g2a*-Myc-His construct was obtained through a gateway reaction with the pDONR221-Pla2g2a entry vector and an engineered destination vector with CMV promoter and MycHisA tag (sPLA2-IIA-myc). Untagged human *Pla2g2a* was cloned into the pCDNA3.1 vector. Human PGRN and granulin-expressing constructs were previously described [53,54]. Mouse *Pla2g2a*-Myc-DDK construct was obtained from Origene (m-sPLA2-IIA-myc). Mouse PGRN construct was cloned into pSecTag2B vector (Invitrogen) with an N-terminal FLAG-His tag (Flag-mPGRN). The N-terminal granulin G and F domains deleted PGRN (PGRNΔGF) (amino acids 206-593) was cloned into the pSectag2A vector with an N-terminal FLAG tag.

Primary Antibodies and Reagents

The following antibodies were used in this study: Rabbit anti-GFP antibody was a gift from Professor Anthony Bretscher; Mouse anti-Myc (9E10) (Sigma, 1:1000 for western blot), mouse anti-GAPDH (Proteintech Group, 1:10000 for western blot), mouse anti-Transferrin (Proteintech Group, 1:1000 for western blot), rat anti-mouse LAMP1 (1D4B) (BD Biosciences, 553793, 1:300 for immunostaining), sheep anti-mouse PGRN (R&D systems, AF2557, 1:750 for western blot), goat anti-CathD (R&D systems, AF1029, 1:100 for immunostaining), sheep anti-mouse sPLA2-IIA (ThermoFisher Scientific, PA5-47672, 1:500 for western blot), rabbit anti-human sPLA2-IIA (Cayman Chemical, 160502, 1:1000 for western blot,1:100 for immunostaining), rabbit anti-IBA-1 (Wako, 01919741, 1:500 for immunostaining), rat anti-CD68 (Bio-Rad, MCA1957, 1:100 for immunostaining), mouse anti-GFAP (Cell signaling, 3670S, 1:100 for immunostaining), mouse anti-ACBD3 (Santa Cruz Biotechnology, sc-101277, 1:200 for immonostaining). Myc-Trap (Chromo Tek), GFP-trap (Proteintech group), Flag-trap (Sigma) were used for anti-myc,anti-GFP, and anti-Flag immunoprecipitations, respectively.

The following reagents were also used in the study: Dulbecco's modified Eagle's medium (DMEM)(Cellgro, 10-017-CV), 0.25% Trypsin (Corning, 25-053-CI), LY333013 (Chemietek, CT-VAREM), KH064 (Millipore Sigma, S3319), Odyssey blocking buffer (LI-COR Biosciences, 927-40000), protease inhibitor (Roche, 05056489001), Pierce BCA Protein Assay Kit (Thermo Scientific, 23225), O.C.T compound (Electron

bioRxiv preprint doi: https://doi.org/10.1101/2023.04.06.535844; this version posted April 6, 2023. The copyright holder for this preprint (which was not certified by peer review) is the author/funder, who has granted bioRxiv a license to display the preprint in perpetuity. It is made available under a CC-BY-NC-ND 4.0 International license.

Microscopy Sciences, 62550-01), Bafilomycin and Chroloquine (Sigma-Aldrich) and mouse sPLA2 activity assay Kit (Cayman Chemical, 765001), human sPLA2-IIA ELISA kit (Cayman Chemical, 501380)

Mouse strains and treatment

Grn$^{-/-}$ mice in the C57/BL6 background[55] mice were obtained from Jackson Labs and housed in the Weill Hall animal facility. These mice were mated to WT FVB mice to generate *Pla2g2a*$^{+/-}$ *Grn*$^{+/-}$ mice. *Pla2g2a*$^{+/-}$ *Grn*$^{+/-}$ mice were bred with each other to generate *Pla2g2a*$^{+/+}$ *Grn*$^{-/-}$ mice. *Pla2g2a* genotyping was performed using the following primers: Forward common, 5'- CAGAGCTGACAGCATGAAGGTCCTC-3'; Reverse WT, 5'-TCTGTGGCATCCTTGGGGGAT-3'; Reverse pla2g2a knockout, 5'- CTGTGGCATCCTTGG GGG AA-3'. The age of the mice used is described in the figure legend for each experiment.

For inhibitor treatment, 5-week-old *Pla2g2a*$^{+/+}$ *Grn*$^{-/-}$ mice were fed with 0.3% DMSO in corn oil, LY333013 (10 mg/kg, dissolved in DMSO and diluted in corn oil) or KH064 (10 mg/kg, dissolved in DMSO and diluted in corn oil) via oral gavage once per day for 3 consecutive weeks. Both male and female mice were included in each group. All the mice were housed in the Weill Hall animal facility at Cornell. All animal procedures have been approved by the Institutional Animal Care and Use Committee (IACUC) at Cornell.

WITHDRAWN
see manuscript DOI for details

Cell Culture and DNA Transfection

HEK293T and Raw 264.7 cells were maintained in Dulbecco's Modified Eagle's Medium (Cellgro) supplemented with 10% fetal bovine serum (Sigma) in a humidified incubator at 37ºC with 5% CO2. Raw 264.7 cells with PGRN deletion or controls were generated as previously described[56]. For transient overexpression, HEK293T Cells were transfected with polyethyleneimine [57].

Protein purification

His-PGRN and sPLA2-IIA protein was purified from the serum-free culture medium of transfected HEK293T cells using cobalt beads. Protein was eluted with imidazole. Purified proteins were further concentrated and changed to PBS buffer using the Centricon device (Millipore).

SILAC and mass spectrometry analysis

HEPG2 cells were grown for a minimum of five generations in DMEM with 10% dialyzed FBS (Sigma) supplemented with either light (C12, N14 arginine, and lysine) or heavy (C13, N15 arginine, and lysine) amino acids. To search for PGRN interactors, the heavy HEPG2 cells were transfected in two 15 cm dishes with GFP-PGRN expression constructs while the light HEPG2 cells were transfected with pEGFP-C1 as a control. Two days after transfection, cells were lysed in 50mM Tris pH8.0, 150mM NaCl, 1% Triton, and 0.1% deoxycholic acid with protease inhibitors (Roche). The lysates were subjected to anti-GFP immunoprecipitation using GFP-Trap beads (ChromoTek). The presence of GFP and GFP-PGRN in immunoprecipitated samples was confirmed by SDS-PAGE and silver staining. Samples were then mixed and boiled for 5 minutes with 1% DTT followed

bioRxiv preprint doi: https://doi.org/10.1101/2023.04.06.535844; this version posted April 6, 2023. The copyright holder for this preprint (which was not certified by peer review) is the author/funder, who has granted bioRxiv a license to display the preprint in perpetuity. It is made available under a CC-BY-NC-ND 4.0 International license.

by alkylation by treating samples with a final concentration of 28 mM iodoacetamide. Proteins were precipitated on ice for 30 minutes with a mixture of 50% acetone/49.9% ethanol/0.1% acetic acid. The protein pellet was washed with the same solution, re-precipitated on ice, and dissolved in 8M urea/50 mM Tris pH 8.0 followed by dilution with three volumes of 50 mM Tris pH 8.0/150 mM NaCl. Proteins were digested overnight at 37º C with 1 µg mass spectrometry grade Trypsin (Promega). The resulting peptide sample was acidified with 10% formic acid and 10% trifluoroacetic acid (TFA) and desalted using a Sep-Pak C18 cartridge (Waters). Samples were eluted with 80% acetonitrile (ACN)/0.1% acetic acid into silanized vials (National Scientific) and evaporated using a SpeedVac. Samples were re-dissolved in 85uL of a solution of ~1% formic acid and 70% can and subject to fractionation via hydrophilic interaction liquid chromatography (HILIC) on an Ultimate 300 LC (Dionex). Each fraction was evaporated with a SpeedVac and resuspended in 0.1% TFA. Samples were subjected to LC-MS/MS analysis using a Q-Exactive mass spectrometer (Thermo Fisher Scientific) and data were analyzed using the SORCERER system (Sage-N Research).

WITHDRAWN
see manuscript DOI for details

Tissue Preparation

Mice were perfused with PBS and tissues were dissected and snap-frozen with liquid nitrogen and kept at -80°C. On the day of the experiment, frozen tissues were thawed and homogenized on ice with bead homogenizer (Moni International) in ice-cold RIPA buffer (150 mM NaCl, 50 mM Tris-HCl [pH 8.0], 1% Triton X-100, 0.5% sodium deoxycholate, 0.1% SDS) with 1 mM PMSF, and 1x protease inhibitors (Roche). After centrifugation at 14,000 × g for 15 minutes at 4℃, supernatants were collected for analysis.

Immunoprecipitation and western blot analysis

Cells were lysed in 50mM Tris pH8.0, 150mM NaCl, 1% Triton, 0.1% deoxycholic acid with protease inhibitors (Roche). The lysates were subject to anti-GFP immunoprecipitation using GFP-Trap beads or anti-Myc immunoprecipitation using Myc-Trap beads (ChromoTek), beads were washed with 50mM Tris pH8.0, 150mM NaCl, 1% Triton after 3-4 hours of incubation. Western Blot was visualized using the Licor-Odyssey system as described[58]. The PGRN and sPLA2-IIA levels in the medium were analyzed following trichloroacetic acid precipitation as described[58].

Immunofluorescence staining, image acquisition, and analysis

For mouse brain section staining, mice were perfused with cold PBS and tissues were post-fixed with 4% paraformaldehyde. After dehydration in 30% sucrose buffer, tissues were embedded in the O.C.T compound (Electron Microscopy Sciences). 20-µm-thick brain sections were cut with cryotome. For paraffin-embedded human brain samples, 8-µm-thick sections were deparaffinized with xylene and ethanol. Antigen retrieval was performed by microwaving in citrate buffer (pH 6.0) for 20 min. Tissue sections were blocked and permeabilized with 0.1% saponin in Odyssey blocking buffer before incubating with primary antibodies overnight at 4℃. The next day, sections were washed 3x with cold PBS followed by incubation with secondary fluorescent antibodies and Hoechst at room temperature for two hours. The slides were then mounted using a mounting medium (Vector laboratories). Images were acquired on a CSU-X spinning disc confocal microscope (Intelligent Imaging

bioRxiv preprint doi: https://doi.org/10.1101/2023.04.06.535844; this version posted April 6, 2023. The copyright holder for this preprint (which was not certified by peer review) is the author/funder, who has granted bioRxiv a license to display the preprint in perpetuity. It is made available under a CC-BY-NC-ND 4.0 International license.

Innovations) with an HQ2 CCD camera (Photometrics) using 63x or 100x objectives, ten to twelve different random images were captured. Lower magnification images were captured by 20x objectives on a Leica DMi8 inverted microscope, three to five images were captured from each sample.

For the quantitative analysis of GFAP, CD68, and IBA1 levels in the brain sections, the fluorescence intensity and area were measured directly using ImageJ after a threshold application. The lipofuscin quantification was determined by the red fluorescence signals (594 nm). For the quantitative analysis of CathD and LAMP1 levels in IBA1-positive microglia, the IBA1-positive microglia were selected. Subsequently, the fluorescence area and intensity of CathD and LAMP1 were measured. Three brain sections per mouse, separated by 100 μm were used for quantification. The mean from the three sections was used to be representative of each mouse. Data from ≥3 brains in each genotype were used for quantitative analysis and normalized to age-matched controls.

WITHDRAWN
see manuscript DOI for details

sPLA2 activity assays

sPLA2 activities were analyzed using a mouse sPLA2 activity assay kit (Cayman Chemical) according to the manufacturer's instructions. Samples were prepared in a 96-well plate and run at 414 nm every minute for 10 min. The activities of recombinant sPLA2-IIA protein (250ng/ml) in the absence or presence of recombinant PGRN or BSA (1250ng/ml or 2500ng/ml) were determined.

PCR with reverse transcription

Total RNAs were extracted using TRIzol (Invitrogen). One microgram of total RNA was reverse transcribed to cDNA using poly (T) primer and SuperScript III Reverse Transcriptase (Invitrogen). Quantitative PCR was performed on a LightCyler 480 (Roch Applied Science), and the transcripts levels were measured using efficiency-adjusted ΔΔ−CT. *Pla2g2a* transcripts were normalized to β-actin. The mouse *Pla2g2a* primer pair sequences were 5′-GGCTGTGTCAGTGCGATAAAXX-3′ and 5′-TTTATCACCGGGAAACTTGG-3′. Mouse β-actin primers were 5′-ACGAGGCCCAGAGCAAGAG-3′ and 5′-TCTCCAAGTCGTCCCAGTTG-3′.

RNA-seq analysis

Total RNA was extracted from cortex regions using Trizol (Thermo scientific). RNA quality was checked using nanodrop, gel electrophoresis, and Agilent Fragment Analyzer. RNAseq libraries were generated by the Cornell TREx Facility using the NEBNext Ultra II Directional RNA Library Prep Kit (New England Biolabs) using 700ng input total RNA per sample. At least 20M reads (2x150nt PE) were generated on a NovaSeq (Illumina). Reads were trimmed to remove low-quality and adaptor sequences with TrimGalore (a wrapper for cutadapt and fastQC), requiring a minimum trimmed length of 50nt. Reads that passed quality control were aligned to reference genome (Ensembl 98.38)[59] using STAR[60], using '--quantMode GeneCounts' to output counts per gene. SARTools[61] and DESeq2[62] were used to generate normalized counts and statistical analysis of differential gene expression. Genes with FDR control p-value ≤ 0.05 and

bioRxiv preprint doi: https://doi.org/10.1101/2023.04.06.535844; this version posted April 6, 2023. The copyright holder for this preprint (which was not certified by peer review) is the author/funder, who has granted bioRxiv a license to display the preprint in perpetuity. It is made available under a CC-BY-NC-ND 4.0 International license.

absolute log fold change ≥ 0.5 were identified as differentially expressed genes (DEGs). Heatmap of the DEGs was generated by using Heatmapper[63]. Gene enrichment analysis using Hallmark and KEGG gene sets was performed using Gene Set Enrichment Analysis (GSEA)[64]. The list of inflammation genes was obtained from GSEA hallmark gene sets and previously published papers. The list of lysosome genes is obtained from GSEA KEGG gene sets.

Statistical analysis

All statistical analyses were performed using GraphPad Prism 8. All data are presented as mean ± SEM. Statistical significance was assessed by unpaired Student's t-test (for two groups comparison) or one-way ANOVA tests with Bonferroni's multiple comparisons (for multiple comparisons). P values less than or equal to 0.05 were considered statistically significant. *$p < 0.05$; **$p < 0.01$.

WITHDRAWN
see manuscript DOI for details

Declarations

Ethical Approval and Consent to Participate

All applicable international, national, and/or institutional guidelines for the care and use of animals were followed. The work under animal protocol 2017-0056 is approved by the Institutional Animal Care and Use Committee at Cornell University.

Consent for publication

All authors have given consent for publication.

Data availability

All data needed to evaluate the conclusions in the paper are present in the paper and/or the Supplementary Materials.

Competing interests

Cornell University has filed a patent application (9987-01-US) for methods using sPLA2-IIA inhibition to treat FTLD-*GRN* and other neurodegenerative diseases.

Funding

This work is supported by NINDS/NIA (R01NS088448 & R01NS095954) to FH and Weill Institute Fleming fellowship to CY. The funders are not involved in the study.

Authors' contributions

H.D. performed SILAC, confirmed the interaction, and demonstrated that sPLA2-IIA expression modifies PGRN deficiency phenotypes and the effect of sPLA2-IIA inhibitors. C.Y determined sPLA2-IIA levels changes in Raw264.7 cells together with H.D., analyzed RNA seq data and lysosome enlargement phenotypes, confirmed the phenotypes in the FVB mice and determined sPLA2-IIA changes in human patient samples. A.L.N provided human patient samples under the guidance of W.S. M. S. helped with mass spec analysis. F.H. supervised the project and wrote the manuscript with H.D. and C.Y.. M.S. edited the manuscript. All authors read and approved the final manuscript.

bioRxiv preprint doi: https://doi.org/10.1101/2023.04.06.535844; this version posted April 6, 2023. The copyright holder for this preprint (which was not certified by peer review) is the author/funder, who has granted bioRxiv a license to display the preprint in perpetuity. It is made available under a CC-BY-NC-ND 4.0 International license.

Acknowledgments

We thank Mrs. Xiaochun Wu for technical assistance; Dr. Eric Boilard (Centre Hospitalier Universitaire de Québec) for helpful discussions and sharing *Pla2g2a* genotyping protocol; Mr. Ethan Sanford for helping with the volcano plot.

WITHDRAWN
see manuscript DOI for details

bioRxiv preprint doi: https://doi.org/10.1101/2023.04.06.535844; this version posted April 6, 2023. The copyright holder for this preprint (which was not certified by peer review) is the author/funder, who has granted bioRxiv a license to display the preprint in perpetuity. It is made available under a CC-BY-NC-ND 4.0 International license.

References:

1. Rhinn, H., Tatton, N., McCaughey, S., Kurnellas, M., and Rosenthal, A. (2022). Progranulin as a therapeutic target in neurodegenerative diseases. Trends Pharmacol Sci *43*, 641-652. 10.1016/j.tips.2021.11.015.
2. Simon, M.J., Logan, T., DeVos, S.L., and Di Paolo, G. (2022). Lysosomal functions of progranulin and implications for treatment of frontotemporal dementia. Trends Cell Biol. 10.1016/j.tcb.2022.09.006.
3. Baker, M., Mackenzie, I.R., Pickering-Brown, S.M., Gass, J., Rademakers, R., Lindholm, C., Snowden, J., Adamson, J., Sadovnick, A.D., Rollinson, S., et al. (2006). Mutations in progranulin cause tau-negative frontotemporal dementia linked to chromosome 17. Nature *442*, 916-919.
4. Cruts, M., Gijselinck, I., van der Zee, J., Engelborghs, S., Wils, H., Pirici, D., Rademakers, R., Vandenberghe, R., Dermaut, B., Martin, J.J., et al. (2006). Null mutations in progranulin cause ubiquitin-positive frontotemporal dementia linked to chromosome 17q21. Nature *442*, 920-924.
5. Gass, J., Cannon, A., Mackenzie, I.R., Boeve, B., Baker, M., Adamson, J., Crook, R., Melquist, S., Kuntz, K., Petersen, R., et al. (2006). Mutations in progranulin are a major cause of ubiquitin-positive frontotemporal lobar degeneration. Hum Mol Genet *15*, 2988-3001.
6. Almeida, M.R., Macario, M.C., Ramos, L., Baldeiras, I., Ribeiro, M.H., and Santana, I. (2016). Portuguese family with the co-occurrence of frontotemporal lobar degeneration and neuronal ceroid lipofuscinosis phenotypes due to progranulin gene mutation. Neurobiol Aging *41*, 200 e201-205. 10.1016/j.neurobiolaging.2016.02.019

S0197-4580(16)00178-0

7. Smith, K.R., Damiano, J., Franceschetti, S., Carpenter, S., Canafoglia, L., Morbin, M., Rossi, G., Pareyson, D., Mole, S.E., Staropoli, J.F., et al. (2012). Strikingly different clinicopathological phenotypes determined by progranulin-mutation dosage. Am J Hum Genet *90*, 1102-1107. 10.1016/j.ajhg.2012.04.021

S0002-9297(12)00254-6

8. Huin, V., Barbier, M., Bottani, A., Lobrinus, J.A., Clot, F., Lamari, F., Chat, L., Rucheton, B., Fluchere, F., Auvin, S., et al. (2020). Homozygous GRN mutations: new phenotypes and new insights into pathological and molecular mechanisms. Brain *143*, 303-319. 10.1093/brain/awz377.
9. Rhinn, H., and Abeliovich, A. (2017). Differential Aging Analysis in Human Cerebral Cortex Identifies Variants in TMEM106B and GRN that Regulate Aging Phenotypes. Cell Syst *4*, 404-415 e405. 10.1016/j.cels.2017.02.009.
10. Nelson, P.T., Dickson, D.W., Trojanowski, J.Q., Jack, C.R., Boyle, P.A., Arfanakis, K., Rademakers, R., Alafuzoff, I., Attems, J., Brayne, C., et al. (2019). Limbic-predominant age-related TDP-43 encephalopathy (LATE): consensus working group report. Brain. 10.1093/brain/awz099.
11. Perry, D.C., Lehmann, M., Yokoyama, J.S., Karydas, A., Lee, J.J., Coppola, G., Grinberg, L.T., Geschwind, D., Seeley, W.W., Miller, B.L., et al. (2013). Progranulin mutations as risk factors for Alzheimer disease. JAMA Neurol *70*, 774-778. 10.1001/2013.jamaneurol.393

1680455 [pii].

12. Sheng, J., Su, L., Xu, Z., and Chen, G. (2014). Progranulin polymorphism rs5848 is associated with increased risk of Alzheimer's disease. Gene *542*, 141-145. 10.1016/j.gene.2014.03.041

S0378-1119(14)00352-7

13. Kamalainen, A., Viswanathan, J., Natunen, T., Helisalmi, S., Kauppinen, T., Pikkarainen, M., Pursiheimo, J.P., Alafuzoff, I., Kivipelto, M., Haapasalo, A., et al. (2013). GRN variant rs5848 reduces plasma and brain levels of granulin in Alzheimer's disease patients. J Alzheimers Dis *33*, 23-27. 10.3233/JAD-2012-120946.

WITHDRAWN
see manuscript DOI for details

bioRxiv preprint doi: https://doi.org/10.1101/2023.04.06.535844; this version posted April 6, 2023. The copyright holder for this preprint (which was not certified by peer review) is the author/funder, who has granted bioRxiv a license to display the preprint in perpetuity. It is made available under a CC-BY-NC-ND 4.0 International license.

14. Xu, H.M., Tan, L., Wan, Y., Tan, M.S., Zhang, W., Zheng, Z.J., Kong, L.L., Wang, Z.X., Jiang, T., Tan, L., and Yu, J.T. (2017). PGRN Is Associated with Late-Onset Alzheimer's Disease: a Case-Control Replication Study and Meta-analysis. Mol Neurobiol *54*, 1187-1195. 10.1007/s12035-016-9698-4.
15. Tayebi, N., Lopez, G., Do, J., and Sidransky, E. (2020). Pro-cathepsin D, Prosaposin, and Progranulin: Lysosomal Networks in Parkinsonism. Trends Mol Med *26*, 913-923. 10.1016/j.molmed.2020.07.004.
16. Rodrigues, P.S., and Kale, P.P. (2021). Mini review - The role of Glucocerebrosidase and Progranulin as possible targets in the treatment of Parkinson's disease. Rev Neurol (Paris). 10.1016/j.neurol.2021.01.015.
17. Nicholson, A.M., Gass, J., Petrucelli, L., and Rademakers, R. (2012). Progranulin axis and recent developments in frontotemporal lobar degeneration. Alzheimers Res Ther *4*, 4. alzrt102

10.1186/alzrt102.
18. Bateman, A., and Bennett, H.P. (2009). The granulin gene family: from cancer to dementia. Bioessays *31*, 1245-1254. 10.1002/bies.200900086.
19. Cenik, B., Sephton, C.F., Kutluk Cenik, B., Herz, J., and Yu, G. (2012). Progranulin: a proteolytically processed protein at the crossroads of inflammation and neurodegeneration. J Biol Chem *287*, 32298-32306. R112.399170
20. Kao, A.W., McKay, A., Singh, P.P., Brunet, A., and Huang, E.J. (2017). Progranulin, lysosomal regulation and neurodegenerative disease. Nat Rev Neurosci *18*, 325-333. 10.1038/nrn.2017.36

nrn.2017.36
21. Zhang, J., Velmeshev, D., Hashimoto, K., Huang, Y.H., Hofmann, J.W., Shi, X., Chen, J., Leidal, A.M., Dishart, J.G., Cahill, M.K., et al. (2020). Neurotoxic microglia promote TDP-43 proteinopathy in progranulin deficiency. Nature. 10.1038/s41586-020-2709-7.
22. Paushter, D.H., Du, H., Feng, T., and Hu, F. (2018). The lysosomal function of progranulin, a guardian against neurodegeneration. Acta Neuropathol *136*, 1-17. 10.1007/s00401-018-1861-8.
23. Zhou, X., Sun, L., Bastos de Oliveira, F., Qi, X., Brown, W.J., Smolka, M.B., Sun, Y., and Hu, F. (2015). Prosaposin facilitates sortilin-independent lysosomal trafficking of progranulin. J Cell Biol *210*, 991-1002. 10.1083/jcb.201502029.
24. Almeida, S., Zhou, L., and Gao, F.B. (2011). Progranulin, a glycoprotein deficient in frontotemporal dementia, is a novel substrate of several protein disulfide isomerase family proteins. PLoS ONE *6*, e26454. 10.1371/journal.pone.0026454

PONE-D-11-12702
25. Murakami, M., Taketomi, Y., Sato, H., and Yamamoto, K. (2011). Secreted phospholipase A2 revisited. J Biochem *150*, 233-255. 10.1093/jb/mvr088.
26. Kim, R.R., Chen, Z., Mann, T.J., Bastard, K., K, F.S., and Church, W.B. (2020). Structural and Functional Aspects of Targeting the Secreted Human Group IIA Phospholipase A2. Molecules *25*. 10.3390/molecules25194459.
27. Dore, E., and Boilard, E. (2019). Roles of secreted phospholipase A2 group IIA in inflammation and host defense. Biochim Biophys Acta Mol Cell Biol Lipids *1864*, 789-802. 10.1016/j.bbalip.2018.08.017.
28. Kennedy, B.P., Payette, P., Mudgett, J., Vadas, P., Pruzanski, W., Kwan, M., Tang, C., Rancourt, D.E., and Cromlish, W.A. (1995). A natural disruption of the secretory group II phospholipase A2 gene in inbred mouse strains. J Biol Chem *270*, 22378-22385. 10.1074/jbc.270.38.22378.
29. Roberson, E.D. (2012). Mouse models of frontotemporal dementia. Ann Neurol *72*, 837-849. 10.1002/ana.23722.
30. Zhu, J., Nathan, C., Jin, W., Sim, D., Ashcroft, G.S., Wahl, S.M., Lacomis, L., Erdjument-Bromage, H., Tempst, P., Wright, C.D., and Ding, A. (2002). Conversion of proepithelin to epithelins: roles of SLPI and elastase in host defense and wound repair. Cell *111*, 867-878.

WITHDRAWN
see manuscript .tex for details

bioRxiv preprint doi: https://doi.org/10.1101/2023.04.06.535844; this version posted April 6, 2023. The copyright holder for this preprint (which was not certified by peer review) is the author/funder, who has granted bioRxiv a license to display the preprint in perpetuity. It is made available under a CC-BY-NC-ND 4.0 International license.

31. Bai, X.H., Wang, D.W., Kong, L., Zhang, Y., Luan, Y., Kobayashi, T., Kronenberg, H.M., Yu, X.P., and Liu, C.J. (2009). ADAMTS-7, a direct target of PTHrP, adversely regulates endochondral bone growth by associating with and inactivating GEP growth factor. Mol Cell Biol *29*, 4201-4219. 10.1128/MCB.00056-09.
32. Guo, F., Lai, Y., Tian, Q., Lin, E.A., Kong, L., and Liu, C. (2010). Granulin-epithelin precursor binds directly to ADAMTS-7 and ADAMTS-12 and inhibits their degradation of cartilage oligomeric matrix protein. Arthritis Rheum *62*, 2023-2036. 10.1002/art.27491.
33. Suh, H.S., Choi, N., Tarassishin, L., and Lee, S.C. (2012). Regulation of progranulin expression in human microglia and proteolysis of progranulin by matrix metalloproteinase-12 (MMP-12). PLoS ONE *7*, e35115. 10.1371/journal.pone.0035115

PONE-D-12-01133
34. Taketomi, Y., Miki, Y., and Murakami, M. (2022). Old but New: Group IIA Phospholipase A2 as a Modulator of Gut Microbiota. Metabolites *12*. 10.3390/metabo12040352.
35. Miki, Y., Taketomi, Y., Kidoguchi, Y., Yamamoto, K., Muramatsu, K., Nishito, Y., Park, J., Hosomi, K., Mizuguchi, K., Kunisawa, J., et al. (2022). Group IIA secreted phospholipase A2 controls skin carcinogenesis and psoriasis by shaping the gut microbiota. JCI Insight *7*. 10.1172/jci.insight.152611.
36. Dore, E., Joly-Beauparlant, C., Morozumi, S., Mathieu, A., Levesque, T., Allaeys, I., Duchez, A.C., Cloutier, N., Leclercq, M., Bodein, A., et al. (2022). The interaction of secreted phospholipase A2-IIA with the microbiota alters its lipidome and promotes inflammation. JCI Insight *7*. 10.1172/jci.insight.152638.
37. Schewe, M., Franken, P.F., Sacchetti, A., Schmitt, M., Joosten, R., Bottcher, R., van Royen, M.E., Jeammet, L., Payre, C., Scott, P.M., et al. (2016). Secreted Phospholipases A2 Are Intestinal Stem Cell Niche Factors with Distinct Roles in Homeostasis, Inflammation, and Cancer. Cell Stem Cell *19*, 38-51. 10.1016/j.stem.2016.05.023.
38. Banfi, D., Moro, E., Bosi, A., Bistoletti, M., Cerantola, S., Crema, F., Maggi, F., Giron, M.C., Giaroni, C., and Baj, A. (2021). Impact of Microbial Metabolites on Microbiota-Gut-Brain Axis in Inflammatory Bowel Disease. Int J Mol Sci *22*. 10.3390/ijms22041623.
39. Padhi, P., Worth, C., Zenitsky, G., Jin, H., Sambamurti, K., Anantharam, V., Kanthasamy, A., and Kanthasamy, A.G. (2022). Mechanistic Insights Into Gut Microbiome Dysbiosis-Mediated Neuroimmune Dysregulation and Protein Misfolding and Clearance in the Pathogenesis of Chronic Neurodegenerative Disorders. Front Neurosci *16*, 836605. 10.3389/fnins.2022.836605.
40. Wang, G., Daniel, B.M., and DeCoster, M.A. (2005). Role of nitric oxide in regulating secreted phospholipase A2 release from astrocytes. Neuroreport *16*, 1345-1350. 10.1097/01.wnr.0000174403.79020.65.
41. Villanueva, E.B., Little, J.P., Lambeau, G., and Klegeris, A. (2012). Secreted phospholipase A(2) group IIA is a neurotoxin released by stimulated human glial cells. Mol Cell Neurosci *49*, 430-438. 10.1016/j.mcn.2012.02.006.
42. Wang, G., Qian, P., Xu, Z., Zhang, J., Wang, Y., Cheng, S., Cai, W., Qian, G., Wang, C., and Decoster, M.A. (2012). Regulatory effects of the JAK3/STAT1 pathway on the release of secreted phospholipase A(2)-IIA in microvascular endothelial cells of the injured brain. J Neuroinflammation *9*, 170. 10.1186/1742-2094-9-170.
43. Martin, R., Cordova, C., and Nieto, M.L. (2012). Secreted phospholipase A2-IIA-induced a phenotype of activated microglia in BV-2 cells requires epidermal growth factor receptor transactivation and proHB-EGF shedding. J Neuroinflammation *9*, 154. 10.1186/1742-2094-9-154.
44. Hernandez, M., Martin, R., Garcia-Cubillas, M.D., Maeso-Hernandez, P., and Nieto, M.L. (2010). Secreted PLA2 induces proliferation in astrocytoma through the EGF receptor: another inflammation-cancer link. Neuro Oncol *12*, 1014-1023. 10.1093/neuonc/noq078.
45. Lopez-Vales, R., Ghasemlou, N., Redensek, A., Kerr, B.J., Barbayianni, E., Antonopoulou, G., Baskakis, C., Rathore, K.I., Constantinou-Kokotou, V., Stephens, D., et al. (2011). Phospholipase

WITHDRAWN
See manuscript DOI for details

bioRxiv preprint doi: https://doi.org/10.1101/2023.04.06.535844; this version posted April 6, 2023. The copyright holder for this preprint (which was not certified by peer review) is the author/funder, who has granted bioRxiv a license to display the preprint in perpetuity. It is made available under a CC-BY-NC-ND 4.0 International license.

A2 superfamily members play divergent roles after spinal cord injury. FASEB J *25*, 4240-4252. 10.1096/fj.11-183186.

46. Moses, G.S., Jensen, M.D., Lue, L.F., Walker, D.G., Sun, A.Y., Simonyi, A., and Sun, G.Y. (2006). Secretory PLA2-IIA: a new inflammatory factor for Alzheimer's disease. J Neuroinflammation *3*, 28. 10.1186/1742-2094-3-28.
47. Nebel, C., Aslanidis, A., Rashid, K., and Langmann, T. (2017). Activated microglia trigger inflammasome activation and lysosomal destabilization in human RPE cells. Biochemical and biophysical research communications *484*, 681-686. 10.1016/j.bbrc.2017.01.176.
48. Katsnelson, M.A., Lozada-Soto, K.M., Russo, H.M., Miller, B.A., and Dubyak, G.R. (2016). NLRP3 inflammasome signaling is activated by low-level lysosome disruption but inhibited by extensive lysosome disruption: roles for K+ efflux and Ca2+ influx. American journal of physiology. Cell physiology *311*, C83-c100. 10.1152/ajpcell.00298.2015.
49. Weber, K., and Schilling, J.D. (2014). Lysosomes integrate metabolic-inflammatory cross-talk in primary macrophage inflammasome activation. The Journal of biological chemistry *289*, 9158-9171. 10.1074/jbc.M113.531202.
50. Brady, O.A., Martina, J.A., and Puertollano, R. (2018). Emerging roles for TFEB in the immune response and inflammation. Autophagy *14*, 181-189. 10.1080/15548627.2017.1313943.
51. Nabar, N.R., and Kehrl, J.H. (2017). The Transcription Factor EB Links Cellular Stress to the Immune Response. Yale J Biol Med *90*, 301-315.
52. Martinez-Fabregas, J., Prescott, A., van Kasteren, S., Pedrioli, D.L., McLean, I., Moles, A., Reinheckel, T., Poli, V., and Watts, C. (2018). Lysosomal protease deficiency or substrate overload induces an oxidative-stress mediated STAT3-dependent pathway of lysosomal homeostasis. Nat Commun *9*, 5343. 10.1038/s41467-018-07741-6.
53. Hu, F., Padukkavidana, T., Vaegter, C.B., Brady, O.A., Zheng, Y., Mackenzie, I.R., Feldman, H.H., Nykjaer, A., and Strittmatter, S.M. (2010). Sortilin-mediated endocytosis determines levels of the frontotemporal dementia protein, progranulin. Neuron *68*, 654-667. S0896-6273(10)00776-2

10.1016/j.neuron.2010.09.034.

54. Zhou, X., Paushter, D.H., Feng, T., Pardon, C.M., Mendoza, C.S., and Hu, F. (2017). Regulation of cathepsin D activity by the FTLD protein progranulin. Acta Neuropathol *134*, 151-153. 10.1007/s00401-017-1719-5

10.1007/s00401-017-1719-5

55. Yin, F., Banerjee, R., Thomas, B., Zhou, P., Qian, L., Jia, T., Ma, X., Ma, Y., Iadecola, C., Beal, M.F., et al. (2010). Exaggerated inflammation, impaired host defense, and neuropathology in progranulin-deficient mice. J Exp Med *207*, 117-128. jem.20091568

10.1084/jem.20091568.

56. Du, H., Wong, M.Y., Zhang, T., Santos, M.N., Hsu, C., Zhang, J., Yu, H., Luo, W., and Hu, F. (2021). A multifaceted role of progranulin in regulating amyloid-beta dynamics and responses. Life Sci Alliance *4*. 10.26508/lsa.202000874.
57. Vancha, A.R., Govindaraju, S., Parsa, K.V., Jasti, M., Gonzalez-Garcia, M., and Ballestero, R.P. (2004). Use of polyethyleneimine polymer in cell culture as attachment factor and lipofection enhancer. BMC Biotechnol *4*, 23. 1472-6750-4-23

10.1186/1472-6750-4-23.

58. Brady, O.A., Zheng, Y., Murphy, K., Huang, M., and Hu, F. (2013). The frontotemporal lobar degeneration risk factor, TMEM106B, regulates lysosomal morphology and function. Hum Mol Genet *22*, 685-695. 10.1093/hmg/dds475.
59. Zerbino, D.R., Achuthan, P., Akanni, W., Amode, M.R., Barrell, D., Bhai, J., Billis, K., Cummins, C., Gall, A., Giron, C.G., et al. (2018). Ensembl 2018. Nucleic Acids Res *46*, D754-D761. 10.1093/nar/gkx1098.

WITHDRAWN
See manuscript DOI for details

bioRxiv preprint doi: https://doi.org/10.1101/2023.04.06.535844; this version posted April 6, 2023. The copyright holder for this preprint (which was not certified by peer review) is the author/funder, who has granted bioRxiv a license to display the preprint in perpetuity. It is made available under a CC-BY-NC-ND 4.0 International license.

60. Dobin, A., Davis, C.A., Schlesinger, F., Drenkow, J., Zaleski, C., Jha, S., Batut, P., Chaisson, M., and Gingeras, T.R. (2013). STAR: ultrafast universal RNA-seq aligner. Bioinformatics *29*, 15-21. 10.1093/bioinformatics/bts635.
61. Varet, H., Brillet-Gueguen, L., Coppee, J.Y., and Dillies, M.A. (2016). SARTools: A DESeq2- and EdgeR-Based R Pipeline for Comprehensive Differential Analysis of RNA-Seq Data. PLoS One *11*, e0157022. 10.1371/journal.pone.0157022.
62. Love, M.I., Huber, W., and Anders, S. (2014). Moderated estimation of fold change and dispersion for RNA-seq data with DESeq2. Genome Biol *15*, 550. 10.1186/s13059-014-0550-8.
63. Babicki, S., Arndt, D., Marcu, A., Liang, Y., Grant, J.R., Maciejewski, A., and Wishart, D.S. (2016). Heatmapper: web-enabled heat mapping for all. Nucleic Acids Res *44*, W147-153. 10.1093/nar/gkw419.
64. Subramanian, A., Tamayo, P., Mootha, V.K., Mukherjee, S., Ebert, B.L., Gillette, M.A., Paulovich, A., Pomeroy, S.L., Golub, T.R., Lander, E.S., and Mesirov, J.P. (2005). Gene set enrichment analysis: a knowledge-based approach for interpreting genome-wide expression profiles. Proc Natl Acad Sci U S A *102*, 15545-15550. 10.1073/pnas.0506580102.

WITHDRAWN
see manuscript DOI for details

bioRxiv preprint doi: https://doi.org/10.1101/2023.04.06.535844; this version posted April 6, 2023. The copyright holder for this preprint (which was not certified by peer review) is the author/funder, who has granted bioRxiv a license to display the preprint in perpetuity. It is made available under a CC-BY-NC-ND 4.0 International license.

Figure Legends

Fig. 1: **Physical interactions between PGRN and sPLA2-IIA.** (**A**) Schematic illustration of the SILAC experiment searching for PGRN interactors in HEPG2 cells. Proteins with more than 4 peptides and p value <0.01 and Log2 (GFP/GFP-PGRN) ratio <-1 were labeled in green. (**B**) Human PGRN and sPLA2-IIA interact when overexpressed in HEK293T cells. Human sPLA2-IIA-myc and human PGRN expressing constructs were transfected into HEK293T cells as indicated. Lysates and conditioned medium were prepared 3 days later and immunoprecipitated with anti-Myc antibodies. (**C**) Mouse-sPLA2-IIA-myc and FLAG-mouse-PGRN expressing constructs were transfected into HEK293T cells as indicated. Lysates and conditioned medium were prepared 3 days later and immunoprecipitated with anti-Myc antibodies. (**D**) Human PGRN interacts with human sPLA2-IIA through granulin F and G. Human-sPLA2-IIA-myc and GFP-PGRN / granulin constructs were transfected into HEK293T cells as indicated. Lysates were prepared 2 days later and immunoprecipitated with GFP-Trap. (**E**) Diagram of PGRN structure. (**F**) Deletion of granulin F and G reduces the interaction between PGRN and sPLA2-IIA. Untagged human sPLA2-IIA and Flag-PGRN / Flag-PGRNΔGF constructs were transfected into HEK293T cells as indicated. Lysates and conditioned medium were collected 2 days later and immunoprecipitated with anti-FLAG antibodies.

WITHDRAWN
See manuscript DOI for details

Fig. 2. PGRN downregulates sPLA2-IIA activities and extracellular sPLA2-IIA levels. (**A**) PGRN inhibits sPLA2-IIA activities *in vitro*. Recombinant sPLA2-IIA protein was incubated with substrates in the absence or presence of recombinant PGRN at a 1:1 or 1:2 molar ratio and sPLA2-IIA activities were measured. (**B, C**) Control and PGRN deficient Raw264.7 cells were cultured in a serum-free medium for 24 hours before the lysates and conditioned media (CM) were harvested. Recombinant PGRN protein was added to the medium at 5ug/ml when indicated. Proteins from the CM were precipitated with TCA. Cell lysates and TCA precipitated medium were blotted with anti-sPLA2-IIA-antibodies. The levels of sPLA2-IIA in the cell lysate and medium were quantified and normalized to GAPDH and transferrin, respectively. The value in PGRN deficient conditions was then normalized to that in the control cells. (**D**) *Pla2g2a* mRNA levels are not affected by PGRN loss. mRNAs were extracted from control and PGRN-deficient Raw264.7 cells. The mRNA levels of sPLA2-IIA were quantified by RT-qPCR and normalized to β-actin. Data are presented as mean ± SEM from three independent experiments. *, $p<0.05$; **, $p<0.01$, Student's t-test (for two groups comparison) or one-way ANOVA tests (for multiple comparisons).

Fig. 3: **PGRN deficiency in the sPLA2-IIA expressing background leads to early glial activation and lipofuscin accumulation.** (**A**) Immunostaining of GFAP, CD68, and IBA1 and auto-fluorescent lipofuscin signals in brain sections from 2-month-old *Pla2g2a*$^{+/+}$ and *Pla2g2a*$^{+/+}$ *Grn*$^{-/-}$ mice. Representative images from the cortex were shown for GFAP/CD68/IBA1 staining and images from the thalamus were shown for lipofuscin signals. Scale bar =100 μm (GFAP/CD68/IBA1); Scale bar =10 μm (Lipofuscin images). (**B**) Quantification of GFAP, CD68, and IBA1 levels and auto-fluorescent lipofuscin signals for the experiment in (a). Data are

bioRxiv preprint doi: https://doi.org/10.1101/2023.04.06.535844; this version posted April 6, 2023. The copyright holder for this preprint (which was not certified by peer review) is the author/funder, who has granted bioRxiv a license to display the preprint in perpetuity. It is made available under a CC-BY-NC-ND 4.0 International license.

presented as mean ± SEM from 5 mice of mixed sexes per group (n=5). 3 brain sections were analyzed for each mouse brain. **, p<0.01, Student's t-test.

Fig. 4. Gene expression changes caused by PGRN deficiency in the sPLA2-IIA expressing background. (**A, B**) Total RNAs were extracted from the cortex of 5-month-old *Pla2g2a*$^{+/+}$ and *Pla2g2a*$^{+/+}$*Grn*$^{-/-}$ mice and the RNA-seq was performed to analyze gene expression changes (n=3). Differential expressed genes (DEGs) with FDR P ≤ 0.05, absolute Log2FC ≥ 0.5 between *Pla2g2a*$^{+/+}$ and *Pla2g2a*$^{+/+}$*Grn*$^{-/-}$ groups are plotted using Heatmapper (A; Upregulated in *Grn*$^{-/-}$; B: downregulated in *Grn*$^{-/-}$). Inflammation genes and lysosomal genes are highlighted in red and green, respectively. (**C**) GSEA pathway analysis of the upregulated pathways with NES (normalized enrichment score)>1.0, NOM p-val (nominal p-value)<0.05, and FDR q-val (false discovery rate q value)<0.25 in RNA samples from the cortex of *Pla2g2a*$^{+/+}$ *Grn*$^{-/-}$ mice compared to these from *Pla2g2a*$^{+/+}$ mice.

Fig. 5. Lysosomal changes caused by PGRN deficiency in the sPLA2-IIA expressing background. (**A, B**) Immunostaining of Cathepsin D (CathD), LAMP1, and IBA1 in brain sections from 2-month-old *Pla2g2a*$^{+/+}$ and *Pla2g2a*$^{+/+}$ *Grn*$^{-/-}$ mice. Representative images from the cortex were shown. CathD and LAMP1 signals in IBA1-positive microglia were quantified. 3 sections per mouse brain and 3 mouse brains were used for each genotype. 10-12 cells per section were analyzed. Scale bar =10 μm. n=3, **, p<0.01. (**C**) Immunostaining of CathD, GFAP, and NeuN in brain sections from 2-month-old *Pla2g2a*$^{+/+}$ and *Pla2g2a*$^{+/+}$ *Grn*$^{-/-}$ mice. Representative images from the cortex were shown. Similar results were obtained from 3 mouse brains. Scale bar=8μm

Fig. 6: **Inhibition of sPLA2-IIA pathway rescues glia activation and lipofuscin accumulation in PGRN deficient mice**. 5-week-old *Pla2g2a*$^{+/+}$ and *Pla2g2a*$^{+/+}$ *Grn*$^{-/-}$ mice were treated with corn oil control or PLA2-IIA inhibitors, LY333013 or KH064 for 3 weeks. (**A**) Brain sections were immunostained with anti-GFAP, CD68, and IBA1 antibodies, and representative images from the cortex region were shown (Scale bar=100 μm). Another set of brain sections was stained with Hoechst and auto-fluorescent lipofuscin signals (red) in the thalamus region were imaged (scale bar=10μm). (**B**) Quantification of GFAP, CD68, and IBA1 levels and auto-fluorescent lipofuscin signals for the experiment in (A). Data are presented as mean ± SEM from five mice per group (n=5). 3 sections were analyzed for each mouse brain. *, p<0.05; **, p<0.01, one-way ANOVA.

Fig. 7: **Inhibition of sPLA2-IIA pathway rescues lysosomal enlargement in PGRN deficient mice.** 5-week-old *Pla2g2a*$^{+/+}$ and *Pla2g2a*$^{+/+}$ *Grn*$^{-/-}$ mice were treated with corn oil control or PLA2-IIA inhibitors, LY333013 or KH064 for 3 weeks. (**A**) Brain sections were immunostained with anti-CathD, NeuN, and IBA1 antibodies, and representative images from the cortex region were shown (Scale bar=10 μm). (**B**) CathD signals in IBA1 positive microglia and NeuN positive neurons were quantified. 10-20 confocal images were randomly captured from each brain section. Ten to twenty microglia and fifty to sixty neurons were quantified per section. 3 sections were analyzed for each mouse brain. Data are presented as mean ± SEM from 3-4 mice per group (n=3-4). *, p<0.05; **, p<0.01, one-way ANOVA.

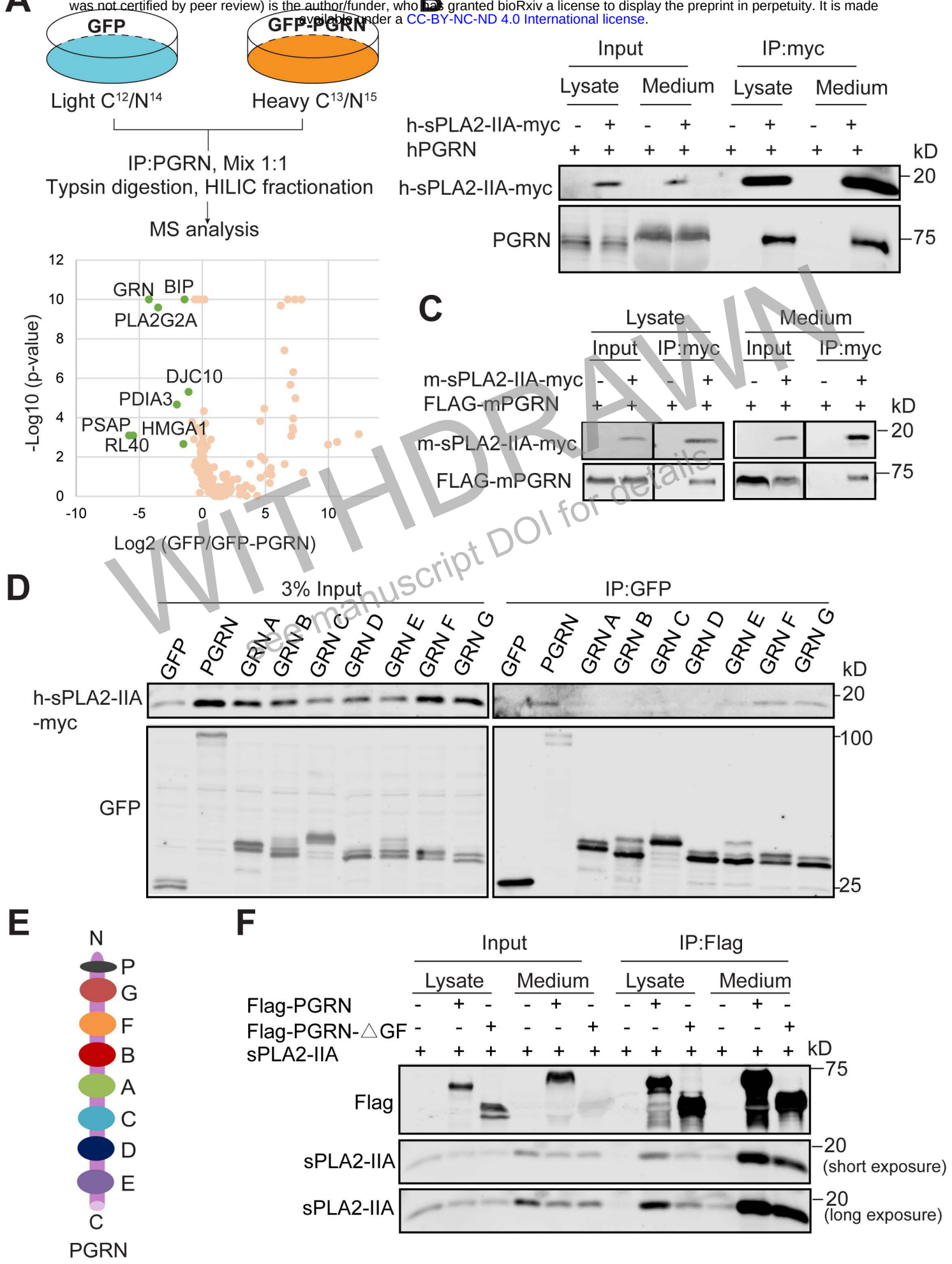
WITHDRAWN
See manuscript DOI for details

bioRxiv preprint doi: https://doi.org/10.1101/2023.04.06.535844; this version posted April 6, 2023. The copyright holder for this preprint (which was not certified by peer review) is the author/funder, who has granted bioRxiv a license to display the preprint in perpetuity. It is made available under a CC-BY-NC-ND 4.0 International license.

Fig. 8: **The levels of sPLA2-IIA are upregulated in FTLD patients with *GRN* mutations**. (**a**) sPLA2-IIA levels were measured in the lysates from postmortem human brain tissues from healthy controls and FTLD with *GRN* mutations or Tau aggregation using ELISA. Data are presented as mean ± SEM from 4-6 cases per group (n=4-6). *, $p<0.05$, Student's t-test. (**b**) Anterior orbital gyrus tissues from healthy controls and FTLD-*GRN* patients were immunostained with anti-sPLA2-IIA and GFAP antibodies. Representative confocal images from 3 different cases for each genotype were shown (Scale bar=10 μm).

WITHDRAWN
see manuscript DOI for details

bioRxiv preprint doi: https://doi.org/10.1101/2023.04.06.535848 this version posted April 6, 2023. The copyright holder for this preprint (which was not certified by peer review) is the author/funder, who has granted bioRxiv a license to display the preprint in perpetuity. It is made available under a CC-BY-NC-ND 4.0 International license.



WITHDRAWN
see manuscript DOI for details

Fig. 1

bioRxiv preprint doi: https://doi.org/10.1101/2023.04.06.535844; this version posted April 6, 2023. The copyright holder for this preprint (which was not certified by peer review) is the author/funder, who has granted bioRxiv a license to display the preprint in perpetuity. It is made available under a CC-BY-NC-ND 4.0 International license.

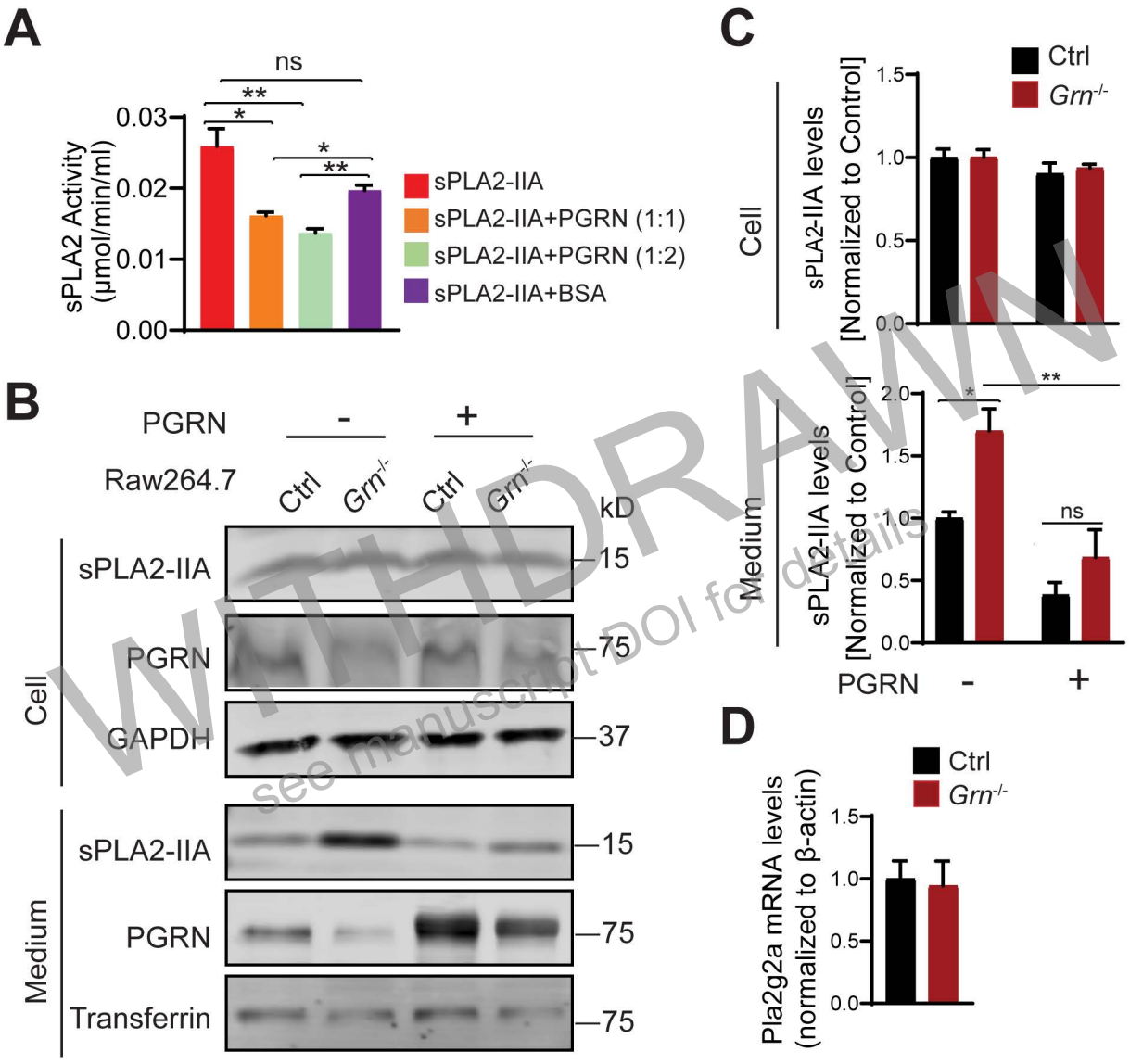
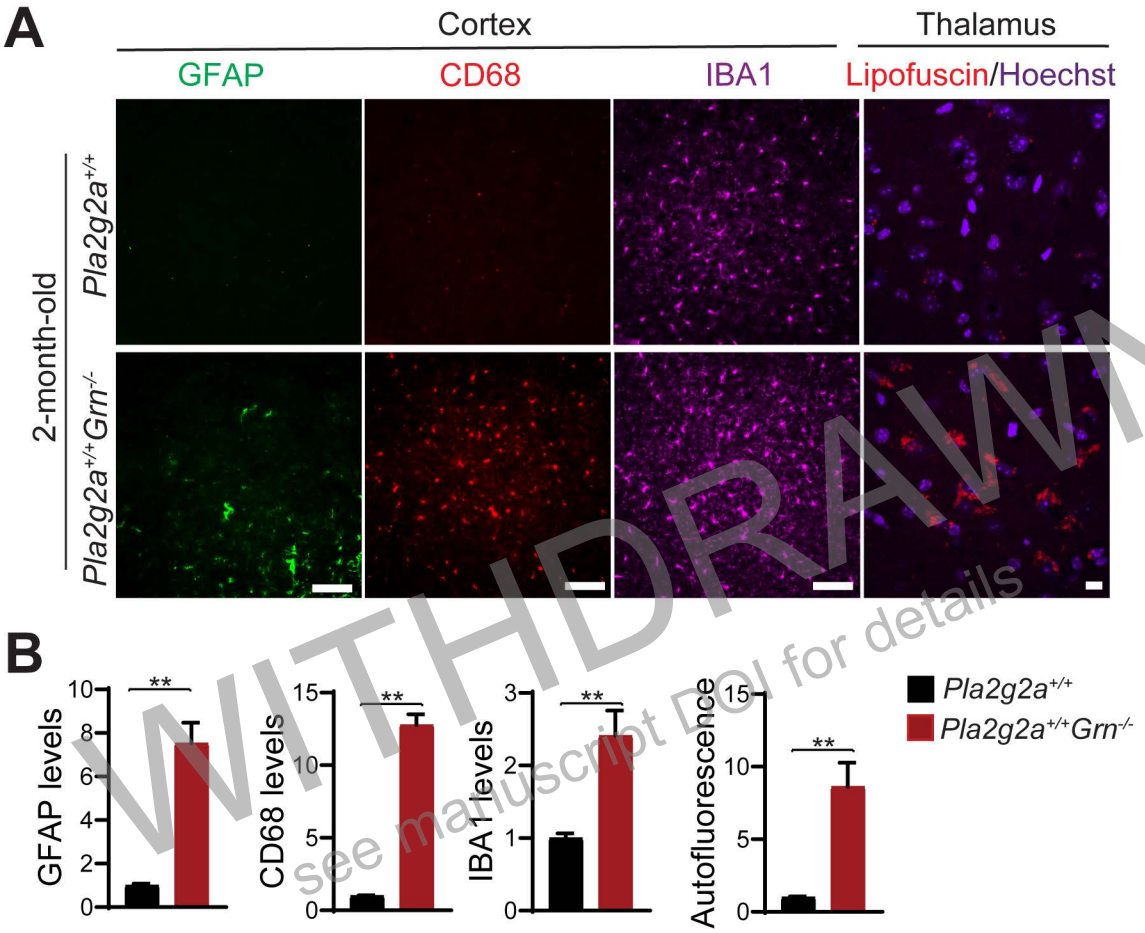


Fig. 2

WITHDRAWN
see manuscript DOI for details

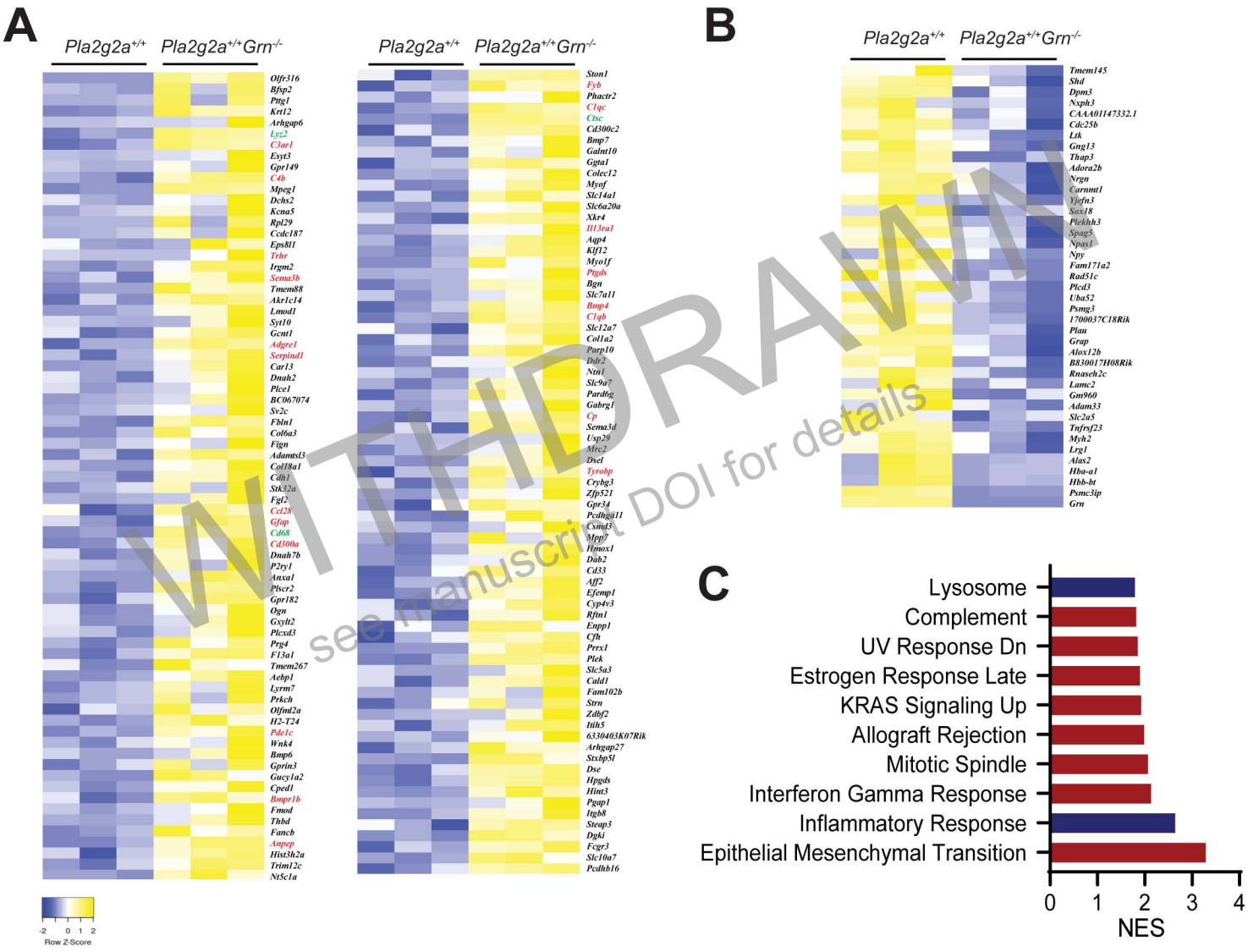
bioRxiv preprint doi: https://doi.org/10.1101/2023.04.06.535844; this version posted April 6, 2023. The copyright holder for this preprint (which was not certified by peer review) is the author/funder, who has granted bioRxiv a license to display the preprint in perpetuity. It is made available under a CC-BY-NC-ND 4.0 International license.



WITHDRAWN
see manuscript DOI for details

Fig. 3

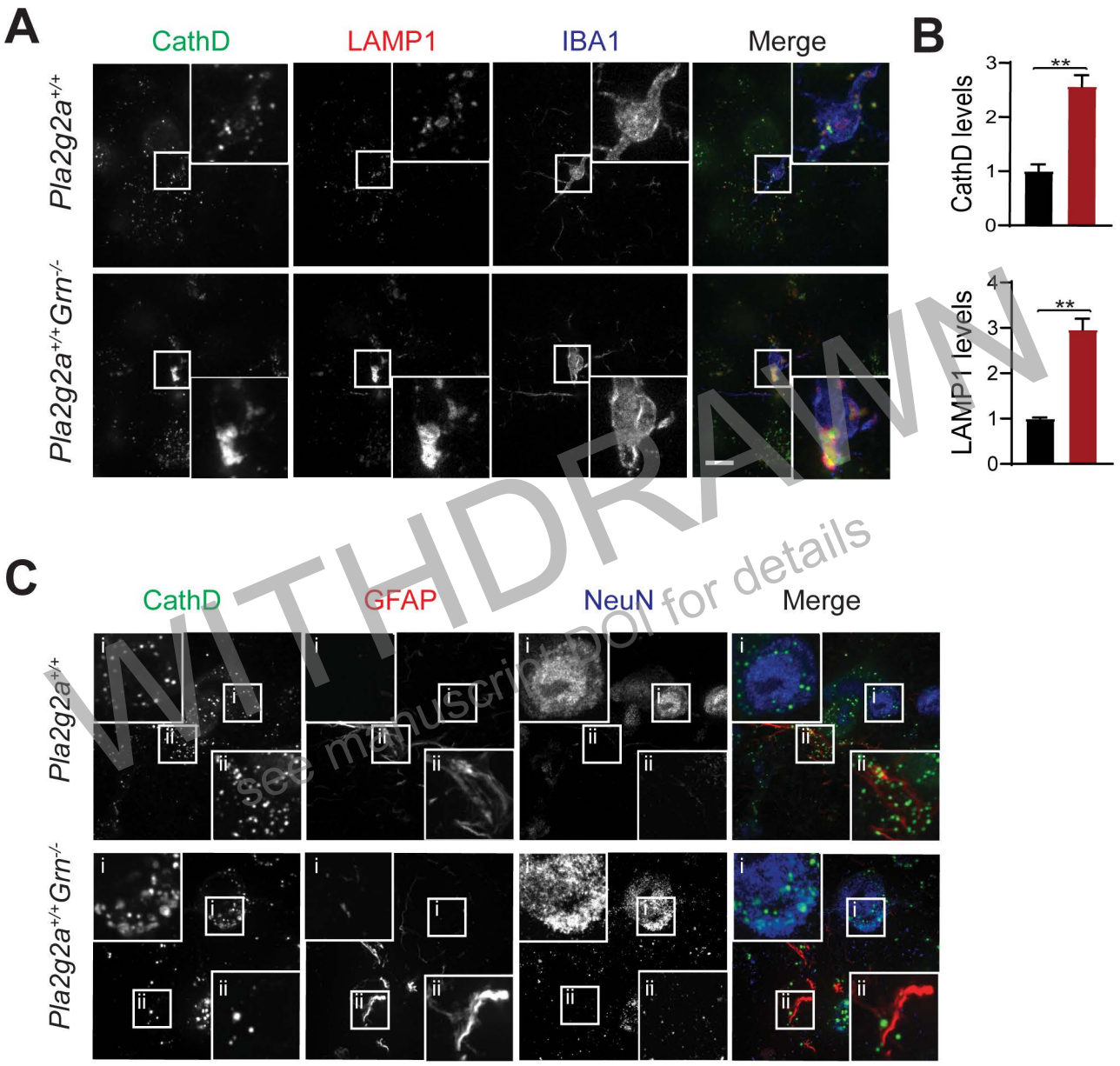
bioRxiv preprint doi: https://doi.org/10.1101/2023.04.06.535844; this version posted April 6, 2023. The copyright holder for this preprint (which was not certified by peer review) is the author/funder, who has granted bioRxiv a license to display the preprint in perpetuity. It is made available under a CC-BY-NC-ND 4.0 International license.



WITHDRAWN
see manuscript DOI for details

Fig.4

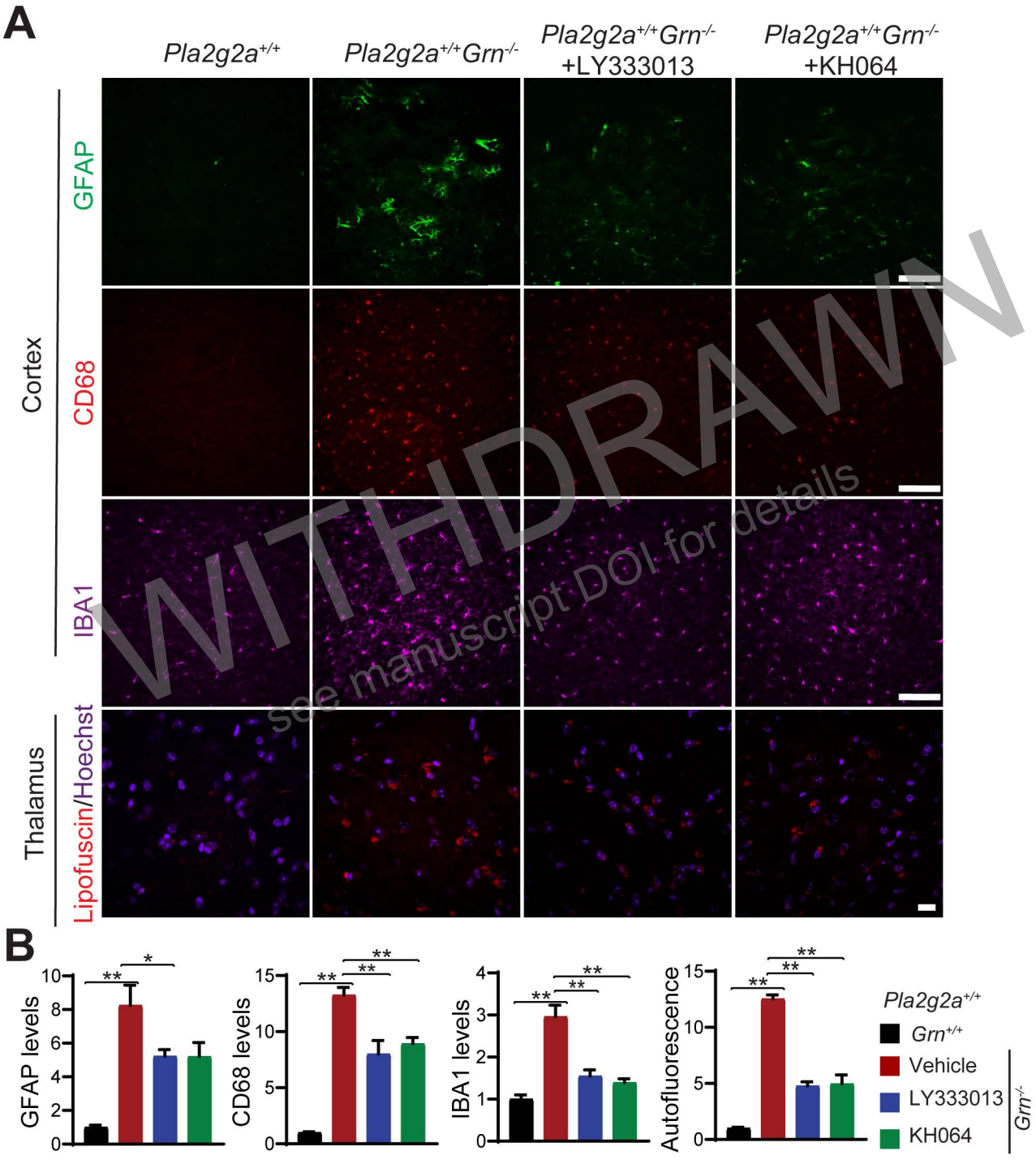
bioRxiv preprint doi: https://doi.org/10.1101/2023.04.06.535844; this version posted April 6, 2023. The copyright holder for this preprint (which was not certified by peer review) is the author/funder, who has granted bioRxiv a license to display the preprint in perpetuity. It is made available under a CC-BY-NC-ND 4.0 International license.



WITHDRAWN
see manuscript pol for details

Fig.5

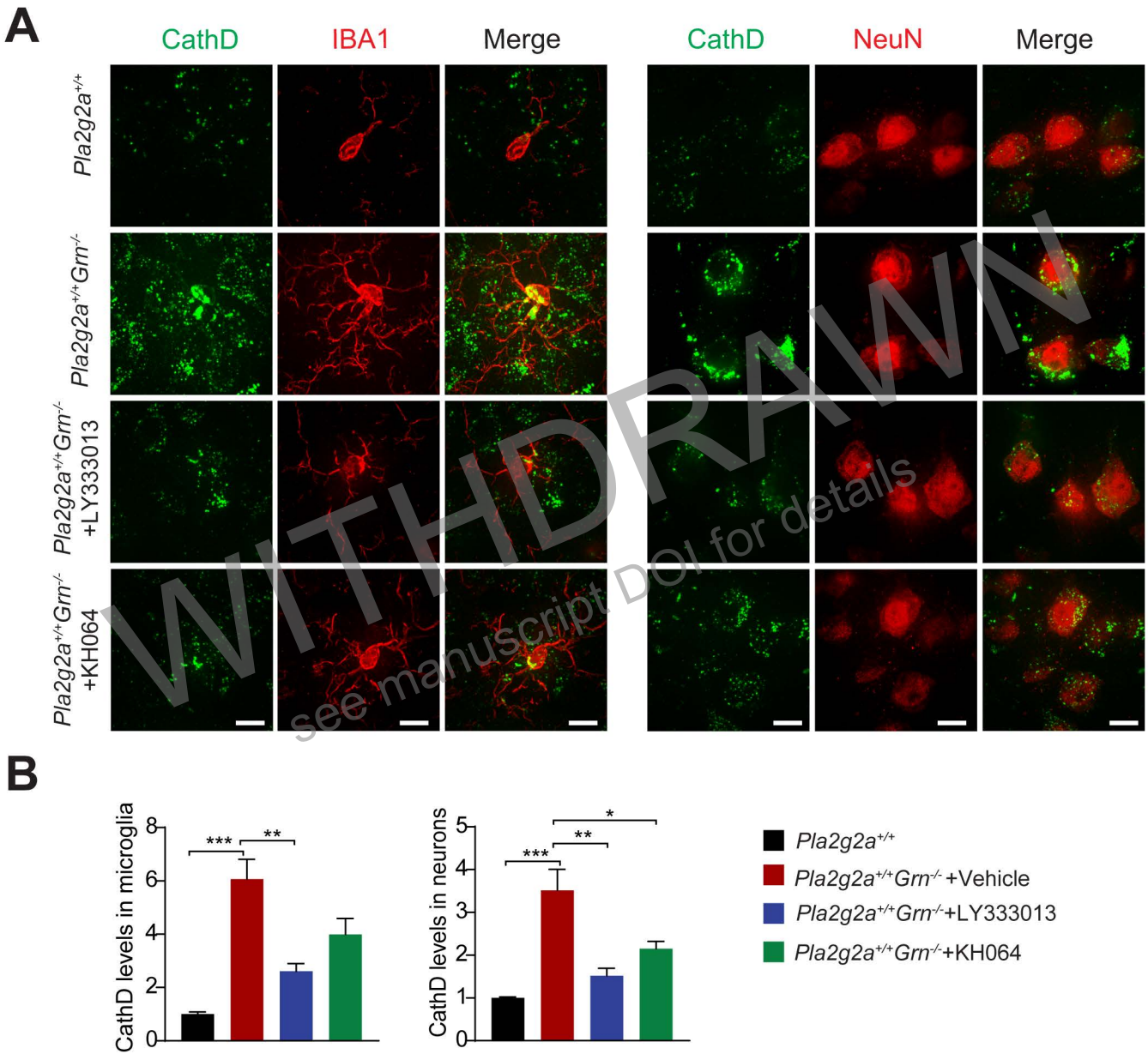
bioRxiv preprint doi: https://doi.org/10.1101/2023.04.06.535844; this version posted April 6, 2023. The copyright holder for this preprint (which was not certified by peer review) is the author/funder, who has granted bioRxiv a license to display the preprint in perpetuity. It is made available under a CC-BY-NC-ND 4.0 International license.



WITHDRAWN
see manuscript DOI for details

Fig.6

bioRxiv preprint doi: https://doi.org/10.1101/2023.04.06.535844; this version posted April 6, 2023. The copyright holder for this preprint (which was not certified by peer review) is the author/funder, who has granted bioRxiv a license to display the preprint in perpetuity. It is made available under a CC-BY-NC-ND 4.0 International license.



WITHDRAWN
see manuscript DOI for details

Fig.7

bioRxiv preprint doi: https://doi.org/10.1101/2023.04.06.535844; this version posted April 6, 2023. The copyright holder for this preprint (which was not certified by peer review) is the author/funder, who has granted bioRxiv a license to display the preprint in perpetuity. It is made available under a CC-BY-NC-ND 4.0 International license.

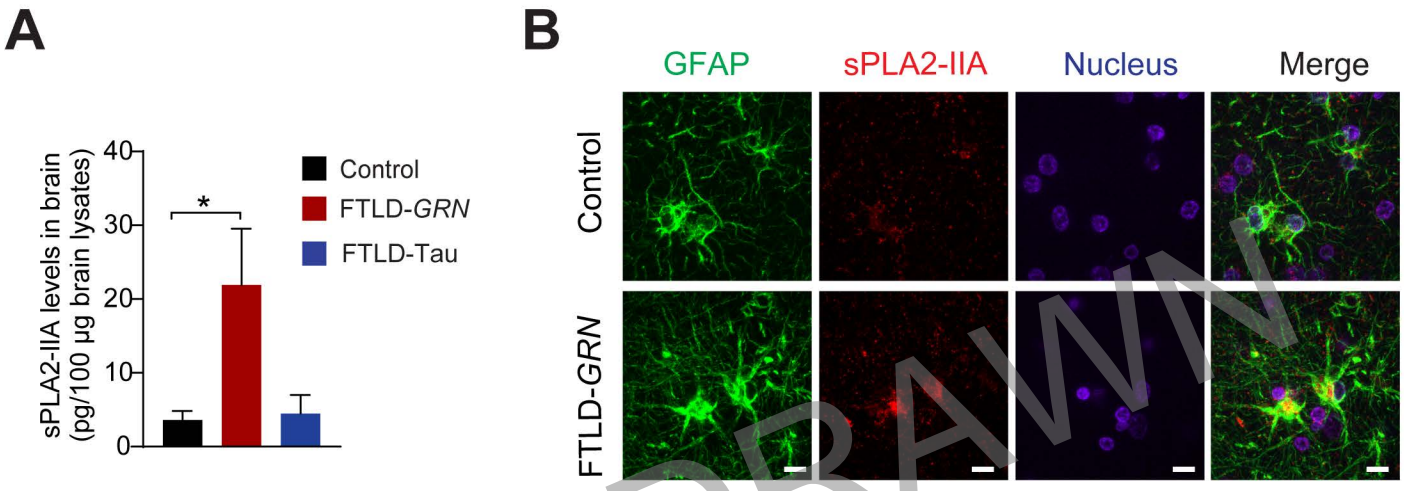


Fig. 8

WITHDRAWN
see manuscript DOI for details